Electronic Structures of Single-Walled Carbon Nanotubes Determined by NMR

X.-P. Tang,[1] A. Kleinhammes,[1] H. Shimoda,[1] L. Fleming,[1] K. Y. Bennoune,[1] S. Sinha,[1] C. Bower,[1] O. Zhou,[1,2] Y. Wu[1,2]*

Single-walled carbon nanotubes were studied by ^{13}C nuclear magnetic resonance (NMR). Two types of ^{13}C nuclear spins were identified with different spin-lattice relaxation rates. The fast-relaxing component, assigned to metallic tubes, followed the relaxation behavior expected in metals, and the density-of-states at the Fermi level increased with decreasing tube diameter. The slow-relaxing component has a significantly lower density-of-states at the Fermi level. Exposure to oxygen has a substantial effect on relaxation rates of both components.

Single-walled carbon nanotubes (SWNTs) have novel electronic properties. For instance, it was predicted theoretically (*1, 2*) that a SWNT can be either metallic or semiconducting depending on its diameter and chirality. Recent scanning tunneling microscopy (STM) and scanning tunneling spectroscopy (STS) measurements (*3, 4*) on individual SWNTs support this prediction. However, the chirality distribution in a bulk sample and its dependence on synthesis conditions are not known. The density-of-states (DOS) at the Fermi level, $g(E_F)$, and its dependence on tube diameters remain to be determined experimentally. Furthermore, the influence of ambient conditions on the properties of SWNTs needs to be investigated because of the openness of the structure. Because NMR probes the local $g(E_F)$, ^{13}C NMR could provide detailed information on $g(E_F)$, the chirality distribution, and the influence of ambient conditions on the properties of SWNTs.

Here, we report a ^{13}C NMR study of SWNTs. Two types of tubes are identified in SWNT samples. One has a relatively short ^{13}C spin-lattice relaxation time (T_1) that follows a temperature dependence characteristic of metals; the estimated value of $g(E_F)$ is comparable to the theoretical value. The other type of tube has a significantly longer T_1, but the associated $g(E_F)$ appears to be finite also. The percentage of the fast- versus slow-relaxing component depends on catalysts used in the synthesis. Exposure to oxygen has a substantial effect on T_1.

SWNT bundles were synthesized by ablating a graphite target containing metal catalysts, using a Nd:YAG (Nd:yttrium-aluminum-garnet) laser operating at a wavelength of 1064 nm (1000 mJ/pulse) in an Ar-filled (200 standard cm^3/min and 93kPa) furnace at 1150°C (*5*). Three types of materials were synthesized using targets with either 0.6 atomic % (each) Ni/Co, 0.3 atomic % Ni/Co, or 2.4 atomic % Rh/Pd under otherwise identical conditions. Samples made with Ni/Co catalysts were purified by a two-step process (*6*) consisting of reflux in 20% H_2O_2 solution at 100°C for 12 hours (with subsequent rinsing in CS_2 and then in methanol) and then filtering through a membrane with 2-μm pores. X-ray diffraction (XRD) and transmission electron microscopy (TEM) (*7*) measurements indicate that the purified samples contain >90% SWNT bundles. Of samples A, B, and C, only sample C was not purified. All the samples were 10% ^{13}C enriched and were annealed at 1100°C for 1 hour in 6.7×10^{-4} Pa vacuum before being sealed under vacuum in glass tubes for NMR measurements.

Figure 1 shows the XRD results and intensity simulations (*8*), which indicate that the average nanotube diameter is 1.40 and 1.32 nm for samples made with 0.6 atomic % Ni/Co (sample A) and 0.3 atomic % Ni/Co (sample B), respectively. No crystalline diffraction pattern was observed in the sample prepared with Rh/Pd catalysts (sample C), indicating a smaller bundle diameter and/or higher packing disorder of the tubes in bundles. Raman spectra are also shown in Fig. 1. The SWNT radial breathing mode is shifted from 172 cm^{-1} in sample A to 258 cm^{-1} in sample C. The Raman shift indicates an average tube diameter of 0.85 nm in sample C (*9*).

Figure 2 shows the static and magic-angle-spinning (MAS) ^{13}C spectra of sample C at room temperature (*10*). The MAS spectrum shows an isotropic shift of 124 ppm with respect to tetramethylsilane (TMS) (*11*). The line shape shows a typical powder pattern of a second-rank tensor with principal axis values of σ_{11} = 195 ppm, σ_{22} = 160 ppm, and σ_{33} = 17 ppm. Such values are characteristic of chemical shift tensors for aromatic carbons. The MAS spectra of samples synthesized using Ni/Co catalysts are similar to that shown in Fig. 2. However, the static spectra are broader because of broadening caused by residual Ni and Co magnetic particles (*7*).

Figure 3 shows a typical saturation recovery curve for sample A. Here, $M^*(t) = 1 - M(t)/M(\infty)$ (M is the magnetization of ^{13}C nuclei) is plotted versus the recovery time (t) at 288 K. $M^*(t)$ can be fit very well with a double-exponential function

$$M^*(t) = \alpha\exp(-t/T_{1\alpha}) + (1-\alpha)\exp(-t/T_{1\beta}) \quad (1)$$

with fitting parameters $\alpha = 0.33 \pm 0.07$, $T_{1\alpha} = 12.0 \pm 0.5$ s, and $T_{1\beta} = 99 \pm 2$ s. This decay curve of double-exponential function is obeyed over the entire temperature range of measurements. Both $1/T_{1\alpha}$ and $1/T_{1\beta}$ are proportional to the temperature (Fig. 4), consistent with Korringa relaxation (*12*). Thus, the

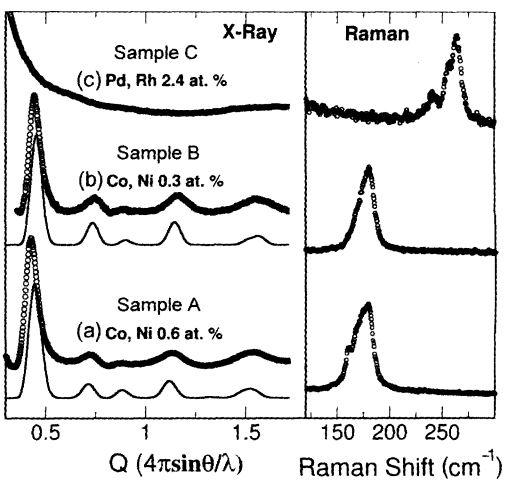

Fig. 1. (Left) Experimental and simulated powder XRD patterns of the three SWNT samples. All three spectra were collected using a two-dimensional imaging plate detector under the same conditions and are presented after background subtraction (*7*). The spectra were simulated based on a two-dimensional triangular lattice composed of uniform diameter SWNTs (*5, 8*) with the diameter and the lattice constant as adjustable variables. Simulations show that the average tube diameters in samples A and B are 1.40 and 1.32 nm, respectively. (Right) The Raman spectra from the same samples collected using 514-nm laser light and a micro-Raman spectrometer with a charge-coupled device detector. The average peak positions of the SWNT breathing mode are 172, 175, and 258 cm^{-1} in samples A, B, and C, respectively. Breathing mode at 258 cm^{-1} in sample C corresponds to an average tube diameter of 0.85 nm (*9*).

[1]Department of Physics and Astronomy and [2]Curriculum in Applied and Materials Sciences, University of North Carolina, Chapel Hill, NC 27599–3255, USA.

*To whom correspondence should be addressed. E-mail: yuewu@physics.unc.edu

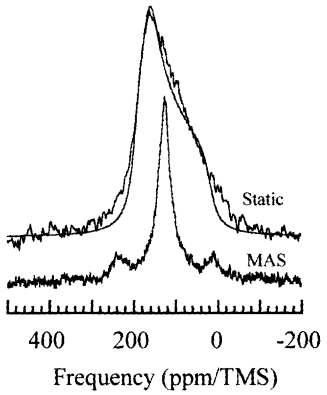

Fig. 2. The static and MAS (spun at 11.7 kHz) ^{13}C spectra of sample C. The isotropic shift is 124 ppm based on the MAS spectrum. The fit is the powder pattern of a chemical shift tensor with σ_{11} = 195 ppm, σ_{22} = 160 ppm, and σ_{33} = 17 ppm.

relaxation is attributed to couplings of ^{13}C with conduction electron spins through the hyperfine interaction (*13*).

On the basis of the theoretical understanding of SWNTs (*1, 2*), the fast-relaxing component is attributed to tubes with indices (*m, n*) where $m - n = 3 \times$ integer, shown theoretically to be metallic. Quantitative evaluation of $g(E_F)$ in such tubes can be obtained by comparison with the NMR result in K_3C_{60} (*14*), where $1/T_1$ of ^{13}C in the normal state of K_3C_{60} was dominated by the dipole-dipole interaction between the electron spins of the ppπ bonding and the ^{13}C spins (*15–17*). This interaction is expected to be even more dominant over other hyperfine interactions (for example, the Fermi-contact interaction) in SWNTs because of the smaller curvature of SWNTs compared to the C_{60} molecule. The relaxation rate, which depends on the orientation of the *z*-axis of the $2p_z$ orbital with respect to the external magnetic field, is given by (*15–17*)

$$\left\langle \frac{1}{TT_1} \right\rangle_{avg} = \frac{2\pi k_B}{\hbar} A_{dip}^2 g^2(E_F) \qquad (2)$$

after averaging over all orientations. Here, $A_{dip} = \frac{2}{5}\gamma_e\gamma_n\hbar^2\left\langle \frac{1}{r^3} \right\rangle$ is the hyperfine coupling constant, where $\langle\ \rangle$ indicates the average over the ppπ orbital, r is the position of the electron with respect to the nucleus, and γ_e and γ_n are the gyromagnetic ratios of the electron spin and the observing nuclear spin, respectively. Ab initio calculation of A_{dip} for K_3C_{60} gives $A_{dip} = 8.2 \times 10^{-7}$ eV (*15*). Because the wave functions at E_F in both K_3C_{60} and SWNTs are predominantly ppπ orbitals, the A_{dip} value in K_3C_{60} is adopted for SWNTs. The value of $\left\langle \frac{1}{TT_1} \right\rangle_{avg}$ for the fast-relaxing component can be estimated as $1/TT_{1\alpha} = 0.00028\ K^{-1}\ s^{-1}$ in sample A (*18*). Thus, Eq. 2 leads to $g(E_F)$ = 0.022 states/(eV·spin·atom) in sample A. Errors could arise from the uncertainty in A_{dip}, which remains to be calculated for SWNTs. The value of $g(E_F)$ in a metallic SWNT is predicted to be inversely proportional to its diameter (*19*). The average diameter (1.4 nm) of the SWNTs in sample A is comparable to that of the (10,10) armchair SWNTs (1.38 nm). The calculated $g(E_F)$ = 0.015 states/(eV·spin·atom) for (10,10) armchair SWNTs (*19*) is comparable to the experimental value. For zigzag and chiral metallic SWNTs, a small curvature-induced gap was predicted to open at E_F (*20*). This gap is about 4 meV for SWNTs of 1.4 nm diameter (*21*). For this NMR study, conducted near and above 200 K, thermal energy smears out such a small gap. Thus, for all metallic SWNTs of similar diameter, the averaged DOS around E_F should be similar to that of armchair SWNTs (*21*). Because of the small value of $g(E_F)$ in metallic SWNTs, the Knight shift is very small compared to the chemical shift effect. Naturally, the slow-relaxing component is attributed to tubes with $m - n \neq 3 \times$ integer, shown theoretically to be semiconducting (*1, 2*). However, the linear temperature dependence of $1/T_{1\beta}$ seems to imply that the corresponding $g(E_F)$ is finite with $g(E_F)$ = 0.0077 states/(eV·spin·atom) in sample A (using $A_{dip} = 8.2 \times 10^{-7}$ eV). Since $T_{1\beta}$ is quite long, other relaxation mechanisms might contribute to the relaxation. Further experimental clarification is needed.

Figure 3 also shows $M^*(t)$ of samples B and C at T = 288 K. The fast-relaxing impurity contribution in sample C with T_1 = 0.5 s is subtracted from this curve. Fitting with double-exponential functions yields $\alpha = 0.36 \pm 0.08$, $T_{1\alpha} = 9 \pm 2$ s, and $T_{1\beta} = 52 \pm 6$ s in sample B, and $\alpha = 0.7 \pm 0.1$, $T_{1\alpha} = 8 \pm 1$ s, and $T_{1\beta} = 60 \pm 10$ s in sample C. The temperature dependence of $1/T_{1\alpha}$ and $1/T_{1\beta}$ of sample C was also measured and was found to be proportional to the temperature as well (Fig. 4). Here, $1/TT_{1\alpha} = 0.00040\ K^{-1}\ s^{-1}$, and the corresponding $g(E_F)$ is 0.026 states/(eV·spin·atom). For the slow-relaxation component, $g(E_F)$ = 0.010 states/(eV·spin·atom) in sample C. The general trend is that $T_{1\alpha}$ decreases with decreasing tube diameter, but more data and better accuracy are needed to determine the precise diameter dependence of $g(E_F)$. The values of $\alpha \approx 1/3$ in samples A and B are consistent with a random chirality distribution, where 1/3 of tubes are metallic with $m - n = 3 \times$ integer. However, since the fast-relaxing component is more than 50% in sample C, it indicates that chirality distribution in SWNT samples is not always random and might be controllable by synthesis conditions (*22*).

Finally, it is worth noting that the relaxation rate changes substantially upon exposure to oxygen, as shown in the inset of Fig. 3. Relaxation rates of nearly all tubes increased dramatically. The most probable mechanism of this effect is the fluctuation of local magnetic field induced by the paramag-

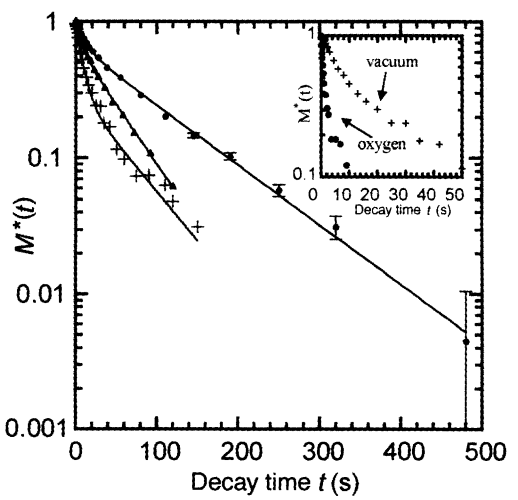

Fig. 3. The $M^*(t)$ is plotted as a function of t at 288 K for samples A (●), B (▲), and C (+). The fits (solid lines) were obtained using Eq. 1. For sample A, error bars larger than the size of the symbols are also shown. The inset shows room-temperature $M^*(t)$ of sample C before (+) and after (●) exposure to oxygen at 159 kPa. Similar effect was observed in samples A and B.

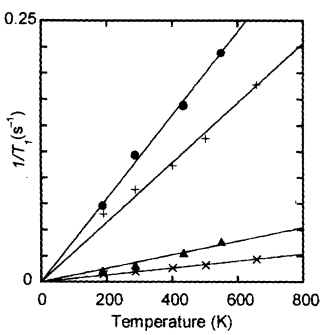

Fig. 4. The temperature dependence of $1/T_{1\alpha}$ for sample A (+) and C (●), and $1/T_{1\beta}$ for sample A (×) and C (▲).

netic oxygen molecules that were strongly attracted to the surfaces of SWNT bundles. However, partial contribution due to possible changes of electronic properties (i.e., they became more metallic) cannot be excluded. This issue is currently under systematic investigation. Nevertheless, interactions between SWNTs and oxygen molecules at room temperature cannot be ignored.

References and Notes

1. J. W. Mintmire, B. I. Dunlap, C. T. White, *Phys. Rev. Lett.* **68**, 631 (1992).
2. R. Saito, M. Fujita, G. Dresselhaus, M. S. Dresselhaus, *Appl. Phys. Lett.* **60**, 2204 (1992).
3. J. W. G. Wildoer, L. C. Venema, A. G. Rinzler, R. E. Smalley, C. Dekker, *Nature* **391**, 59 (1998).
4. T. W. Odom, J.-L. Huang, P. Kim, C. M. Lieber, *Nature* **391**, 62 (1998).
5. A. Thess *et al.*, *Science* **273**, 483 (1996).
6. O. Zhou, B. Gao, C. Bower, L. Fleming, H. Shimoda, *Mol. Cryst. Liq. Cryst.*, in press.
7. Supplemental data, figures, and discussions are available at *Science* Online at www.sciencemag.org/feature/data/1048140.shl
8. T. Yildirim, O. Zhou, J. E. Fischer, *Fullerene-Based Materials*, W. Andreoni, Ed. (Kluwer Academic, Dordrecht, Netherlands, in press).
9. H. Kataura *et al.*, *Jpn. J. Appl. Phys.* **37**, L616 (1998).
10. NMR measurements were done in a field of 9.4 T. The ^{13}C T_1 was measured by the saturation-recovery method with pulsed spin-locking detection. Intensity calibration showed that the observable ^{13}C nuclei are over 80% in sample C. Paramagnetic centers, which might wipe out spins in the surrounding and experimental errors, such as the sample dependence of the Q factor, may contribute to the small discrepancy.
11. The MAS spectra taken at various recovery times after a saturation pulse in sample C reveal a broad featureless peak, which has a short spin-lattice relaxation time of 0.5 s at room temperature. This peak is about 30% of the total intensity and is attributed to impurities in sample C.
12. J. Winter, *Magnetic Resonance in Metals* (Clarendon, Oxford, 1971).
13. Although $T_{1\beta}$ is comparable to the lowest ^{13}C T_1 value observed in graphite (100 to 1000 s at 300 K), the concentration of graphite and carbon nanoparticles in the present sample is too small to account for the observed two-thirds of the ^{13}C nuclear spins. Furthermore, the residual Ni particles are generally wrapped in carbon nanoparticles, which would be wiped out from the NMR signal by local magnetic field. Therefore, ^{13}C nuclei associated with both $T_{1\alpha}$ and $T_{1\beta}$ were attributed to SWNTs.
14. R. Tycko *et al.*, *Phys. Rev. Lett.* **68**, 1912 (1992).
15. V. P. Antropov, I. I. Mazin, O. K. Andersen, A. I. Liechtenstein, O. Jepsen, *Phys. Rev. B* **47**, R12373 (1993).
16. C. H. Pennington *et al.*, *Phys. Rev. B* **53**, R2967 (1996).
17. C. H. Pennington and V. A. Stenger, *Rev. Mod. Phys.* **68**, 855 (1996).
18. The ratio $T_{1\beta}/T_{1\alpha} = 8$ far exceeds the largest ratio of 2.5 between the fastest and the slowest relaxation rate due to the anisotropy of the relaxation mechanism (*16*). Thus, the nonexponential decay is due to the distribution of tube properties, rather than the relaxation mechanism. However, each of the two components can be nonexponential due to the anisotropic relaxation mechanism as well as the distribution of tube diameters. Such details, however, cannot be revealed by data. If the decay is not strictly exponential, $1/T_{1\alpha}$ should be a good estimate of the decay rate at early time, and this is equal to $\langle 1/T_1 \rangle_{avg}$ [see (*16*)].
19. J. W. Mintmire and C. T. White, *Appl. Phys. A* **67**, 65 (1998).
20. C. L. Kane and E. J. Mele, *Phys. Rev. Lett.* **78**, 1932 (1997).
21. J. W. Mintmire and C. T. White, *Phys. Rev. Lett.* **81**, 2506 (1998).
22. Often, the distribution of relaxation rate was described by a stretched exponential function $M^* = \exp[-(t/\tau)^{\beta}]$, although here the double-exponential fit is generally better (*7*). However, both these points of views describe distribution of tube properties and differ only quantitatively in nature.

23. We thank H. Kataura for helpful discussion and J. Lorentzen and L.E. McNeil for assistance in Raman measurement. Supported by the U.S. Office of Naval Research and the NSF.

21 December 1999; accepted 3 March 2000

Crossed Nanotube Junctions

M. S. Fuhrer,[1] J. Nygård,[1] L. Shih,[1] M. Forero,[1] Young-Gui Yoon,[1] M. S. C. Mazzoni,[1] Hyoung Joon Choi,[2] Jisoon Ihm,[2] Steven G. Louie,[1] A. Zettl,[1] Paul L. McEuen[1]*

Junctions consisting of two crossed single-walled carbon nanotubes were fabricated with electrical contacts at each end of each nanotube. The individual nanotubes were identified as metallic (M) or semiconducting (S), based on their two-terminal conductances; MM, MS, and SS four-terminal devices were studied. The MM and SS junctions had high conductances, on the order of 0.1 e^2/h (where e is the electron charge and h is Planck's constant). For an MS junction, the semiconducting nanotube was depleted at the junction by the metallic nanotube, forming a rectifying Schottky barrier. We used two- and three-terminal experiments to fully characterize this junction.

Single-walled carbon nanotubes (SWNTs) have been proposed as an ideal system for the realization of molecular electronics (*1*). Individual SWNTs may act as devices such as field-effect transistors (*2, 3*), single-electron-tunneling transistors (*4, 5*), or rectifiers (*6–10*). However, a question remains: How can individual SWNTs be joined together to form multiterminal devices and, ultimately, complex circuits? We have begun to address this question by characterizing SWNT-SWNT junctions formed by nanotubes that lie across one another on a substrate. This type of junction is easily constructed and, with the development of techniques to place nanotubes with precision on substrates (*11*), could conceivably be mass produced.

Our SWNT-SWNT junctions consist of two crossed individual SWNTs or small bundles (diameter <3 nm) of SWNTs with four electrical contacts, one on each end of each SWNT or bundle (*12*). In addition, a gate voltage V_g can be applied to the substrate to change the charge density per unit length of the SWNTs. In an atomic force microscope (AFM) image of a completed crossed nanotube device (Fig. 1), two crossed SWNTs (green) interconnect the Cr/Au contacts (yellow).

We can independently measure each SWNT and determine its properties in this configuration. SWNTs may be metallic or semiconducting, depending on their chirality (*13*). At room temperature, metallic SWNTs have a finite conductance that is nearly independent of V_g. Semiconducting SWNTs are found to be p-type, conducting at negative V_g and insulating at positive V_g (*2*). Our crossed SWNT can be composed of two metallic SWNTs (MM), one metallic and one semiconducting SWNT (MS), or two semiconducting SWNTs (SS).

The two-terminal conductances measured across MM junctions are comparable to the two-terminal conductances of the individual SWNTs; the junction resistance is of the same order of magnitude as that of the tubes and their metallic contacts. This result prompted us to measure the four-terminal conductances of the crossed SWNT devices in order to accurately determine the junction conductance. Current is passed into one arm of one tube and sunk from one arm of the second tube. The other arms act as voltage probes. Figure 2A shows the four-terminal current-voltage (I-V) characteristic of an MM junction at 200 K (*14*). The slope of IV corresponds to a resistance of 200 kilohm, or a conductance G of 0.13 e^2/h (where e is the electron charge and h is Planck's constant). Similar measurements of three other MM junctions gave conductances of 0.086, 0.12, and 0.26 e^2/h.

The measured conductances of MM junctions correspond to a transmission probability for the junction $T_j = G/(4e^2/h) \approx 0.02$ to 0.06. Thus, an electron arriving at the junction in one SWNT has chance of a few percent of tunneling into the other SWNT. MM junctions make surprisingly good tunnel contacts, despite the extremely small junction area (on the order of 1 nm^2). We have performed first-principles density functional calculations of the conductance of MM junctions (*15*) (see supplementary material

[1]Department of Physics, University of California at Berkeley and Materials Sciences Division, Lawrence Berkeley National Laboratory, Berkeley, CA 94720, USA. [2]Department of Physics and Center for Theoretical Physics, Seoul National University, Seoul 151-742, Korea.

*To whom correspondence should be addressed. E-mail: mceuen@socrates.berkeley.edu